KPAF (K-band phased array feed) instrument concept

Lisa Locke*[a,b], Stéphane Claude[a], Jens Bornemann[b], Doug Henke[a], James Di Francesco[a], Frank Jiang[a], Dominic Garcia[a], Ivan Wevers[a], Pat Niranjanan[a]
[a]NRC Herzberg, 5071 West Saanich Road, Victoria, BC, Canada, V9E 2E7,
[b]University of Victoria, 3800 Finnerty Road, Victoria, BC, Canada, V8P 5C2

ABSTRACT

Astronomical surveys are demanding more throughput from telescope receivers. Currently, microwave/millimeter telescopes with mature cryogenic single pixel receivers are upgrading to multi-pixel receivers by replacing the conventional feed horns with phased array feeds (PAFs) to increase the field of view and, thus, imaging speeds. This step in astronomy instrumentation has been taken by only a few research laboratories world-wide and primarily in L-band (0.7-1.5 GHz). We present a K-band (18-26 GHz) 5x5 modular PAF to demonstrate the feasibility of higher frequency receiving arrays. The KPAF system includes a tapered slot antenna array, a cryogenic commercial GaAs MMIC amplifier block, and a mixing stage to down-convert to L band for an existing beamformer. The noise temperature and power budget are outlined. Full antenna S-parameters and far-field beam patterns are simulated and measured using both planar near-field and far-field techniques. Cryogenic and room temperature amplifier noise measurements with varying bias levels are presented.

Keywords: Array, beamforming, cryogenic, field of view, MMIC, phased array feed (PAF), radio astronomy, tapered slot antenna (TSA)

1. INTRODUCTION

Astronomy large-scale surveys require instrumentation to minimize the time required to complete observations of large sections of the sky. Optimizing receiver systems has historically been achieved by reducing the amount of internally generated noise, the system temperature, by reducing amplifier noise which is fast approaching the quantum noise limit. An alternative is to take advantage of the telescope's imaging capability by using independent feed-receiver systems in the focal plane. Akin to optical CCDs, the densely packed wide beamwidth phased array feed (PAF) elements greatly enlarge the field of view (FoV) while maintaining the Rayleigh resolution. Unlike widely spaced multi-beam horn feeds, in a single observation the densely packed PAF is capable of full Nyquist sampling. The FoV can be increased with additional modular PAF segments adding to the contiguous fully sampled region. Despite higher system temperatures than single pixel feeds, PAFs can achieve faster survey speeds due to the enlarged FoV.

A 5x5 K-band (18-26 GHz) PAF comprising a planar antenna array and receiver has been designed as part of the current effort to increase the field of view of radio astronomy telescopes. This system is a technology demonstrator for its frequency and for its planar substrate antenna design. K-band represents an increase by more than a factor of 10 in frequency from the existing L-band (0.7-1.5 GHz) PAFs and presents a significant yet attainable engineering challenge for PAF antenna and receiver design.

Scientifically, K-band is attractive because it contains numerous molecular transitions, in particular the rotation-inversion lines of ammonia (NH_3). These transitions are excited in dense gas, and can be used to measure directly the kinetic temperatures and velocities of clouds in the process of forming stars throughout the Galaxy. Depending on the line detected, gas of different temperatures can be probed. For instance line (1,1) at 23.694 GHz and (2,2) at 23.723 GHz can be used to probe cold gas below 40 K. Lines (3,3) at 23.87 GHz and (4,4) at 24.139 GHz can be used to probe hotter gas in the 100 K range. In order to identify each hyperfine component within each line, a minimum spectral resolution of 1 km/s (77 kHz at 23 GHz) is needed. Furthermore, the velocities of the medium in which the ammonia is present can shift by up to 1000 km/s, that is 77 MHz. In conclusion, in order to detect in one band these ammonia lines, the minimum IF bandwidth is 600 MHz for a RF centered at 23.9 GHz.

*lsl@uvic.ca

Millimeter, Submillimeter, and Far-Infrared Detectors and Instrumentation for Astronomy VII, edited by Wayne S. Holland, Jonas Zmuidzinas, Proc. of SPIE Vol. 9153, 91531Z · © 2014 SPIE · CCC code: 0277-786X/14/$18 · doi: 10.1117/12.2057146

In order to compare receiver architectures with different system temperatures, number of beams, polarizations and other parameters, it is common practice to use survey speed ratios. This will be used to evaluate our KPAF system at various cryogenic temperatures against the "gold standard" single pixel feed.

The following sections incorporate the design, simulation and measurement of the manufactured single polarization room temperature array and cryogenic receiver system. A synthesized beam is shown and the KPAF system is compared to a single pixel feed system using the proven method of survey speed ratios.

2. SYSTEM DESCRIPTION

A block diagram of the KPAF system including a 5x5 planar antenna array, 5x5 block of 25 dB gain cryogenic MMIC low noise amplifiers (LNAs), and 25 mixers down converting from 18-26 GHz to 0.8-1.5 GHz allowing the use of an existing L-band receiver and beamformer[1] are shown in Figure 1. In order to consider the impact of overall system temperature, T_{sys}, three different configurations have been considered, each with varying physical temperatures, and the first two configurations are built and tested in this work. The first is a room temperature (300 K) antenna and LNA, the second is a room temperature antenna and a cryogenic (13 K) LNA, and the third has a cryogenic antenna and LNA. The loss of the antenna is determined from radiation efficiency calculations to be 0.55 dB and the coaxial line loss is 0.2 dB. The room temperature LNA performance is 26.5 dB gain and 180 K noise temperature, and the cryogenic performance is 30 dB gain and 25 K noise temperature. The calculated T_{sys} for a single antenna element and LNA is shown, and the array T_{sys} is estimated to be 15% higher to account for mutual coupling of the elements[2]. We assume the single antenna element efficiency is the same as the array element efficiency.

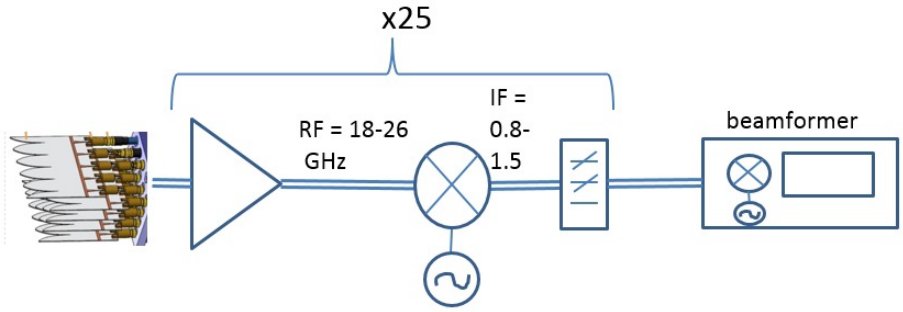

Physical Temperatures		antenna + cable	LNA	Tsys Single	Tsys Array
$T_{ANT} = T_{LNA} = 300K$	Gain/Loss (dB)	-0.75	26.5	270	311
	Noise Temp (K)	57	180		
$T_{ANT} = 300K, T_{LNA} = 13K$	Gain/Loss (dB)	-0.75	30	86	99
	Noise Temp (K)	57	25		
$T_{ANT} = T_{LNA} = 13K$	Gain/Loss (dB)	-0.75	30	32	37
	Noise Temp (K)	2.5	25		

Figure 1. KPAF block diagram showing the antenna array, one of 25 total receiver chains, and the beamformer backend. Three different physical temperature scenarios are outlined. Component gains and losses are used to compute system temperatures. Single and Array Tsys refer to the single antenna element plus receiver system and array plus receiver system. Array Tsys is expected to be 15% higher than single element Tsys[2]. The backend from PHAD[1] will be used for testing.

3. SINGLE ANTENNA

3.1 Description

The tapered slot antenna (TSA) in Figure 2 offers moderate gain, narrow width therefore high spatial density, the possibility of active component integration and symmetric beams in E- and H-planes. The TSA, a type of travelling wave antenna, operates as the electromagnetic wave propagates along the increasingly separated metalized tapers until the distance between the tapers is equal to half the wavelength, allowing wave separation from the antenna structure.[3]

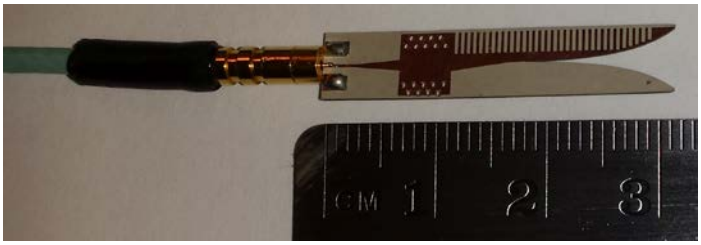

Figure 2. Manufactured 18 – 26 GHz KPAF antenna using Rogers RT/Duroid 6010 substrate with custom Rosenberger coaxial cable with miniSMP connector on antenna side and K-type (2.92 mm) coaxial connector on LNA side (not shown).

Microstrip antennas are inexpensive to fabricate, have narrow profiles, can be integrated with MMIC and coaxial components, and can be easily manufactured into arrays, yet they have lower radiating efficiency due to substrate losses, are physically fragile, and cryogenic cooling is largely untested. The substrate chosen is 0.381 mm (15 mil) Rogers RT Duroid 6010 LM (ε_r = 10.2, tanδ = 0.003 at 20 GHz). The high dielectric permits a $\lambda/2$ element width satisfying the grating lobe condition at the expense of higher noise temperature due to mutual coupling. The thick substrate creates unwanted substrate modes that are eliminated using comb-like corrugations to form an electronic band gap structure cutting off the substrate mode at the operating frequency[4]. Also, thick substrates incur added insertion loss. The loss can be reduced by cutting away the substrate material in the aperture opening using a 355 nm UV laser with a 2 mil kerf and 35 μm beam. The antenna design is the subject of an earlier parametric TSA study.[5]

The antipodal configuration of the top and bottom metallic tapers matches the two-conductor substrate integrated waveguide (SIW). The SIW section allows for a waveguide-like transmission line carrying a TE_{10} mode[6]. Like rectangular waveguide, the SIW can work single-mode from slightly above the cutoff frequency, f_c, to 2 f_c, i.e. 15.1 GHz to 30.2 GHz, easily covering the full K-band. Note there are no TM modes owing to the non-continuous waveguide "walls" by the discrete vias.

This is followed by a tapered microstrip section to standard 50 ohm microstrip line and then a Rosenberger miniSMP connector. Custom Rosenberger RTK Flex405 low loss coaxial cable with miniSMP connector is used on the antenna end and K-type male on the other for connection to the amplifier.

The original design relied on two via holes to provide grounding between the miniSMP connector and the bottom ground plane. During testing, however, it was necessary to improve the grounding by additionally soldering the outer connector shell to the bottom ground plane. This solved the instability problem, dramatically improving the effectiveness of the calibration standards and the KPAF antenna measurements.

Figure 3: Custom triple short (SSST) calibration. Left: calibration standards, top plane. Middle: calibration standards, ground plane. Standards from left to right: Thru, Short1, Short2, Short3. Right: KPAF single antenna with resulting calibration plane noted.

3.2 S-parameter testing results

Vector network analyzer (VNA) measurements using custom triple short (SSST) calibration standards, Short1 = 4.7 mm, Short2 = 5.13 mm, Short3 = 5.65 mm, and Thru = 4.7 mm shown in Figure 3 calibrate out all electrical contributions up to the intersection between SIW and tapered slot antenna marked by a dark line. The measured S_{11} results in Figure 4 show on average similar results compared with frequency and time domain full-wave electromagnetic simulations using ANSYS HFSS v14 and CST Microwave Studio 2014.

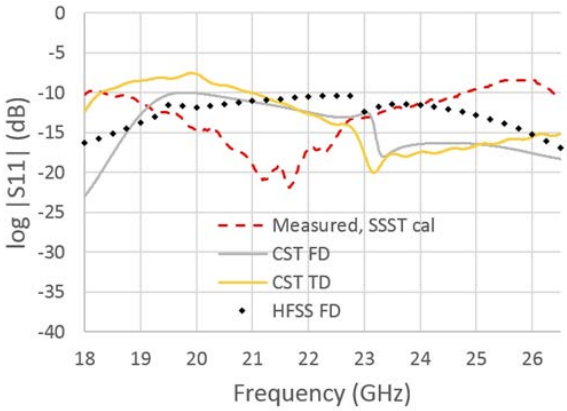

Figure 4. Single KPAF S_{11}, measured vs simulation.

3.3 Radiation pattern testing

Far-field radiation patterns are obtained from planar near-field and far-field techniques pictured in Figure 5. The planar near-field setup includes a Nearfield Systems Inc. (NSI) 0.9 m x 0.9 m planar scanner, a WR42 K-band waveguide probe with variable attenuator scanning the plane in front of the antenna under test (AUT). The separation distance between probe and AUT is chosen to be in between the near-field, $0.62\sqrt{\frac{D^3}{\lambda}}$ and far-field, $2\frac{D^2}{\lambda}$ distance of the AUT to ensure evanescent modes do not significantly contribute to the measured near-field data. The probe distance is set to 155 mm corresponding to a maximum far-field angle of ±70° which proves to be sufficient to measure the E-plane 10 dB beamwidth of 132° at 20 GHz and a slightly wider H-plane 10 dB beamwidth of 140°.

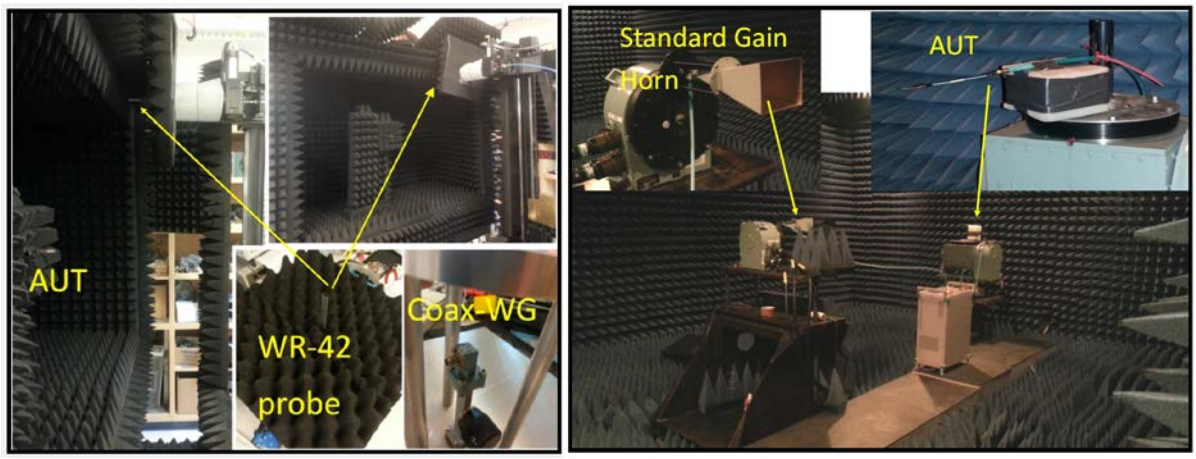

Figure 5. Far-field radiation pattern testing methods: planar near-field scanner (left) and anechoic chamber with far-field scanner (right).

The far-field setup is a large anechoic chamber with an ORBIT/FR Az/El positioner rotating the AUT through 360° in azimuth and 180° in elevation. The stationary 25 dB K-band standard gain horn and an in-line amplifier provide enough gain to overcome the 67 dB free space loss at 26 GHz between the standard gain horn and AUT. The far-field distance, 1.74 m is determined by the standard gain horn's largest dimension, 10 cm.

The near- and far-field scanning measurement and simulation results from Figure 6 for the single KPAF are summarized in Table 1. The CST and HFSS simulated beamwidths agree extremely well. All values are relatively close except those in bold. The planar near-field scanning technique, despite scanning a low-directivity antenna, measures only slightly higher, ~10% off of the beamwidth values than simulations.

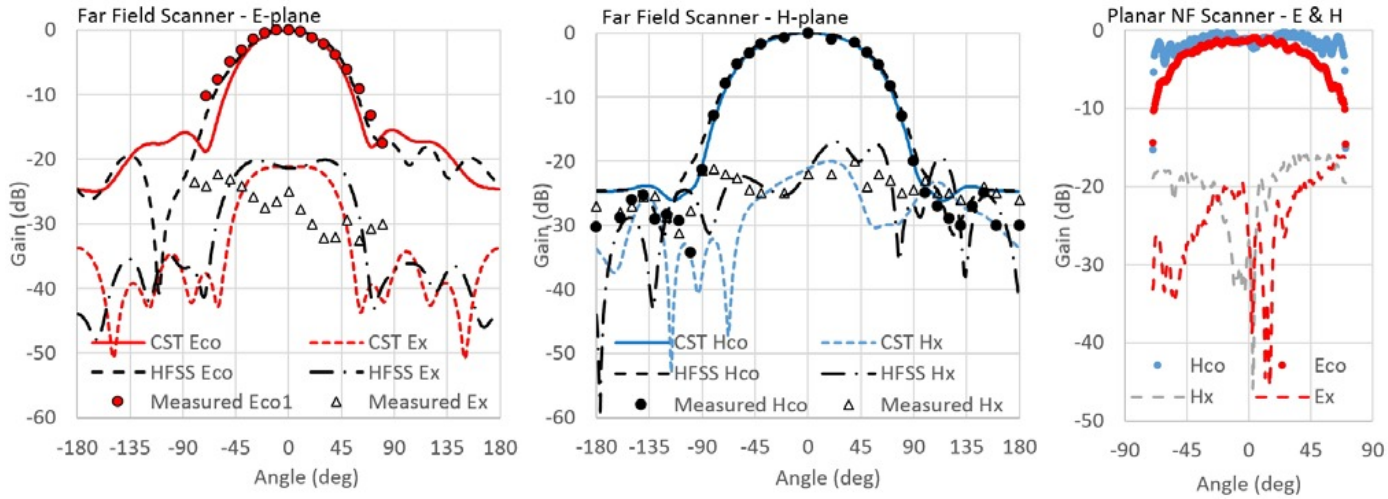

Figure 6. Far-field radiation patterns, single KPAF antenna, normalized to maximum gain (dB). Simulated: CST and HFSS. Measured: far-field scanner (left: E plane, middle: H plane) and planar near-field scanner (right: E and H planes). 20 GHz.

Table 1. Summary of E-plane and H-plane (E/H) 10 dB beamwidths for single KPAF antenna. CST and HFSS simulated values. Near-field scanning (NF) and far-field scanning (FF) measurements. Data farthest from average marked in boldface.

Frequency (GHz)	E-plane				H-plane			
	CST	HFSS	NF	FF	CST	HFSS	NF	FF
18	107	110	**123**	110	140	140	146	145
20	112	112	**132**	**130**	150	152	140	150
22	120	120	-	130	146	147	-	144
26	120	120	-	120	138	137	-	130

3.4 Noise temperature testing results

Simulated results provide radiation efficiency values that we use to estimate the equivalent noise temperature of the antenna. This efficiency, e_{cd} , takes into account the conductor and dielectric losses. A single KPAF antenna efficiency is 0.88 minimum over the frequency band. We calculate the single antenna noise temperature, T_{ant} at a physical temperature 300 K to be

$$T_{ant} = \left(\frac{1}{e_{cd}} - 1 \right) 300\,\mathrm{K} = 40\,\mathrm{K} \tag{1}$$

so that the insertion loss of the antenna is 0.55 dB as used in the system temperature calculations in Section 2.

4. ANTENNA ARRAY

An array is defined by the individual element pattern presented in the previous section, the relative spacing between elements, and the geometrical layout including maximum extent. KPAF is intended for eventual use on the 10 m CART reflector at NRC Herzberg in Penticton with AFAD's L-band down converter and analog beamformer.[1]

4.1 Geometrical parameters

To avoid grating lobes, the maximum element spacing d/λ for an array at the focus of a paraboloidal reflector of half angle θ is[7] $d/\lambda = (1 + \sin\theta)^{-1}$. For a paraboloid with f/D of 0.45, the half angle is $\theta = 58°$, therefore the element spacing at 24 GHz in both x and y planes is $d = 6.2$ mm.

The maximum extent of the array as determined by aberrations due to off-axis feeds within the telescope focal plane, can be calculated using two methods; the first uses classic paraboloidal reflector theory to estimate the maximum radial feed dimension ρ/λ, determined by the off focus location where the axial distance between the flat array and the curved focal arc differs within a given margin of error as shown in Figure 4 of Minnett and Thomas[8]. The resulting maximum array size using this classical radius calculation is 20x20 elements (129 mm x 129 mm). The second, for reflector systems,

Hayman[9] calculates the encircled power in the focal region as a function of focal plane radius, *f/D*, and reflector diameter. The focal plane radius is 40.5 mm at 79 percent encircled power. This corresponds to a maximum array size of 11x11 (71 mm x 71 mm).

The current system is a 5x5 K-band array at element spacing 6.2 mm in both *x* and *y* for an overall size of 31 mm x 31 mm with the future possibility of using this modular block as a subset of a larger 15x15 array (93 mm x 93 mm). The 15x15 array is well within the classical radius calculation limit and with the knowledge that the beamforming will decrease off axis aberrations, is a viable system. Currently, receiver expense and required signal processing systems limit the array to 5x5 elements.

4.2 1x5 Array

Full S-parameters for the 1x5 array in Figure 7 characterize the impedance match, S_{nn}, and degree of mutual coupling between ports, S_{nm} are measured with a VNA with a SSST calibration to move the reference plane up to the intersection between the SIW and antenna section, exactly the same procedure as with the single KPAF antenna in Section 3.2. The results are shown in Figure 8, along with the port numbers

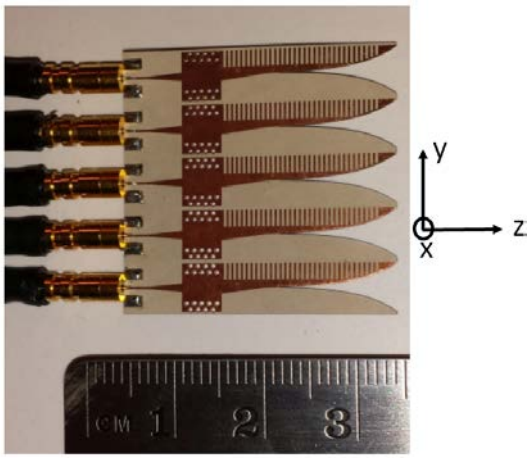

Figure 7. Manufactured 1x5 "blade" array with miniSMP coaxial connectors and cables.

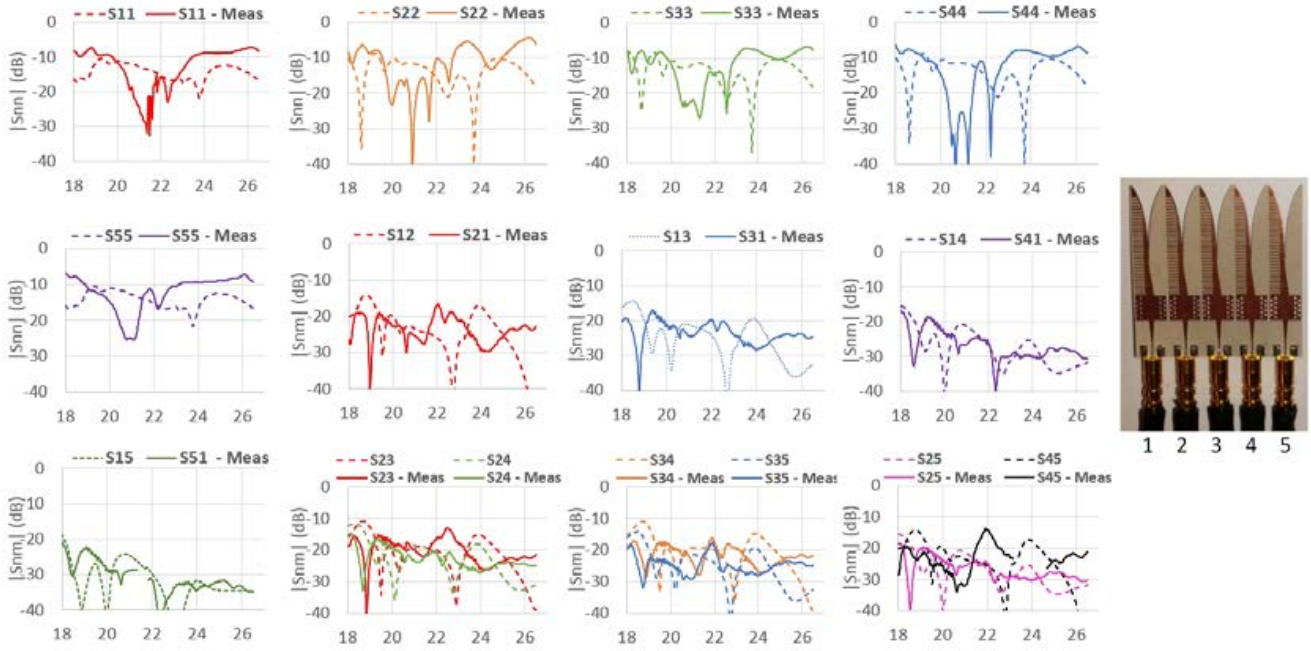

Figure 8. KPAF 1x5 array embedded single element S-parameter results vs frequency (GHz) including input return loss, S_{nn}, and mutual coupling, S_{nm}. Unused ports are terminated in 50Ω coaxial loads. X-axis: frequency (GHz). Simulated (dashed lines) and measured (solid lines). Array port definitions are shown in the inset.

As for the single KPAF element, the far-field radiation patterns of the 1x5 array are also measured with both planar near-field and the far-field scanner setup. Measured and simulated co-polarized gain patterns vs angle for both the E- and H-planes and the simulated cross-polarized gain in the D-plane are shown in Figure 9. There is very good agreement between simulated and measured results.

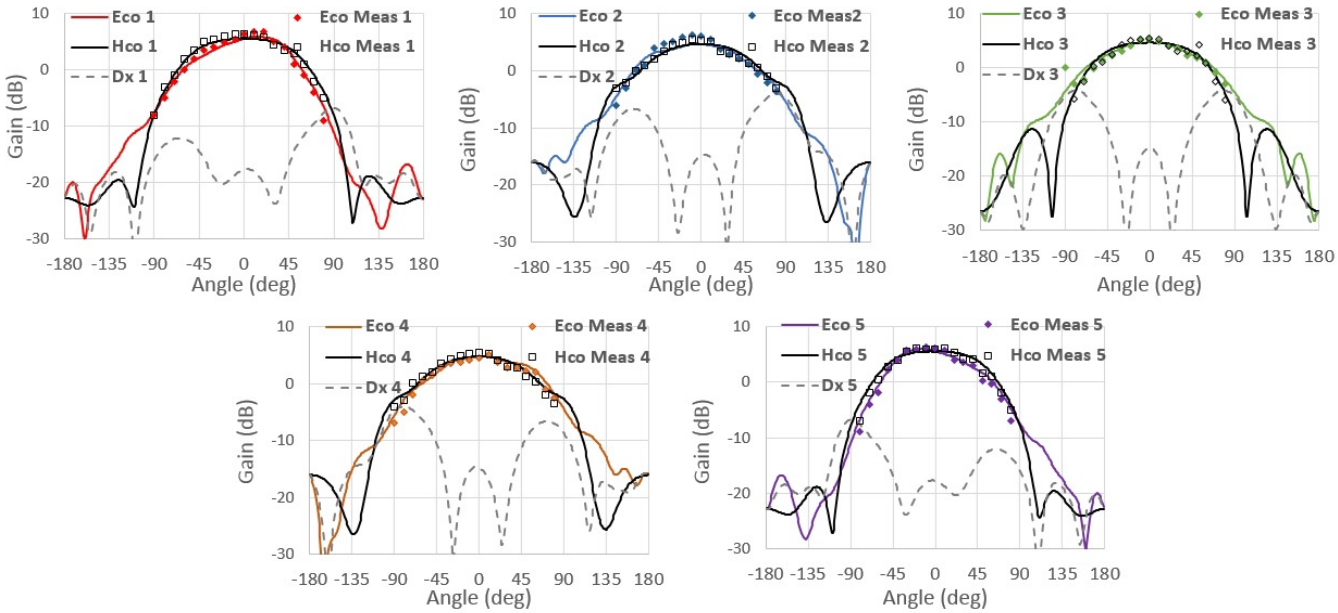

Figure 9. Co-polar (Co) and cross-polar (X) gain (dB) patterns vs θ (deg) of 1x5 KPAF array, simulated and measured with far-field scanner at 22 GHz. E-plane (φ = 90°), H-plane (φ = 0°), D-plane (φ = 45°). Array port definitions as in Figure 8.

4.4 5x5 array

Stacking 5 1x5 "blade" antennas creates the array in Figure 10. Mechanically, the aluminum mounting allows the coaxial cables to be pulled through the plate. Each miniSMP connector is pressed into and locked with its mating 1x5 blade connector. With the five cables attached to the blade, the connector line is lowered into the aluminum mount; when aligned, the cable connector notch slides back into the aluminum mount slot edge. Having the five cable end connectors in place, the aluminum retainer is inserted into the five openings and fastened to the mount with cap screws holding the cable end connectors and blade in place.

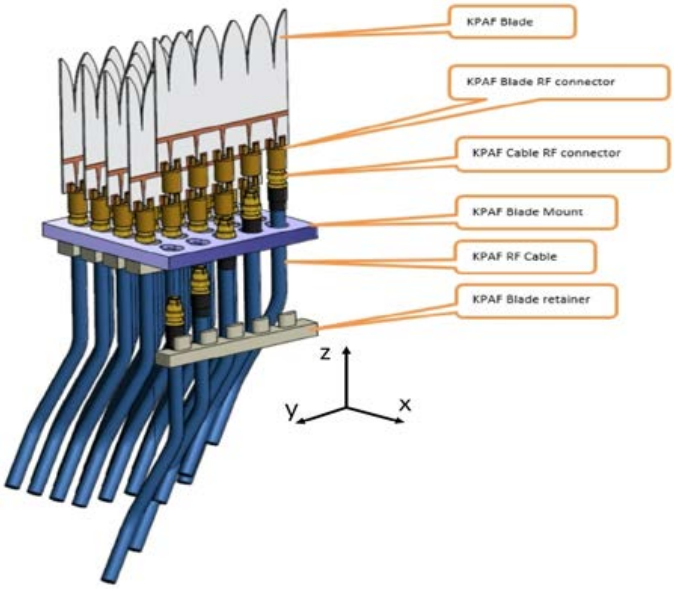

Figure 10. KPAF 5x5 array mechanical mounting design, expanded view.

Figure 11 represents a simulation of the synthesized axially symmetric beam with ring structured element weightings 0 dB, -10 dB, -20 dB for the centre element, first ring and second ring respectively with zero phase weightings. Assuming

a telescope with f/D = 0.45 (resulting in a half angle of 58.1°), a 5x5 PAF can generate a single beam with sufficient aperture efficiency. The lightly weighted outer elements act as a buffer required to provide the centre elements with an appropriate boundary so as to not corrupt the radiation pattern. Optimization of the element weightings is ongoing. This is a first step, and future designs will incorporate the modularity of the 5x5 KPAF to create 10x10 or 15x15 element systems providing many more beams.

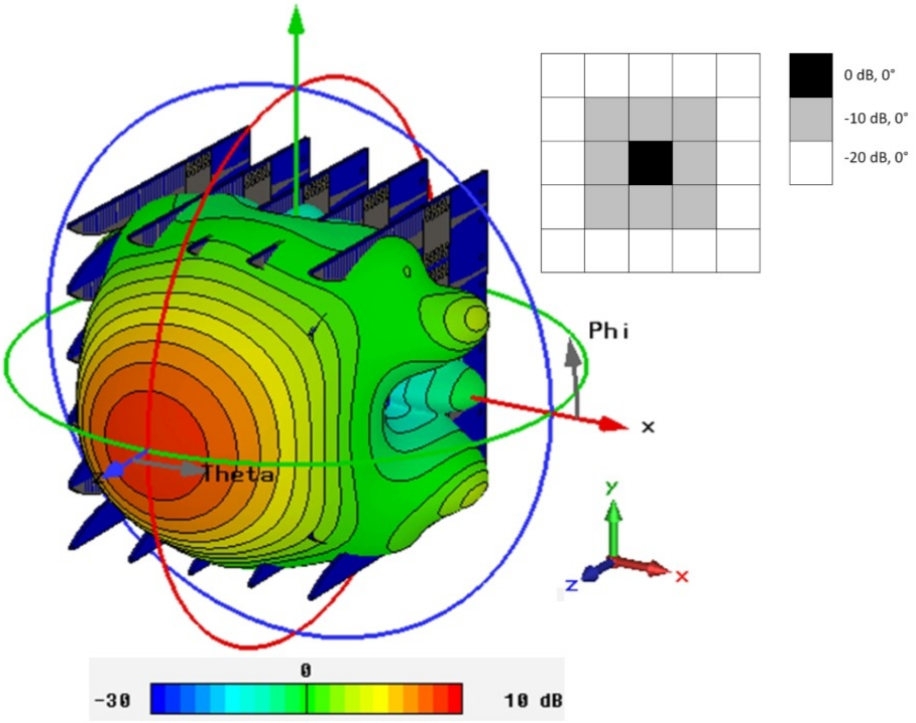

Figure 11. Gain of simulated synthesized beam (dB) of 5x5 array with element amplitude and phase weightings: centre element: 1.0, 0°, inner ring: 0.1, 0°, outer ring: 0.01, 0°. Contours represent 1 dB steps. The physical array structure demonstrates orientation. 22 GHz.

5. RECEIVER

5.1 LNA description

A cryogenic 1x5 amplifier block housing commercial GaAs MMIC amplifier chips (CMD160) was manufactured and tested. The custom MMIC chip is low-noise, low-power and has 50 ohm matched ports, eliminating the need for external DC blocks and RF port matching. The CMD160 chip room temperature performance for 17-25 GHz is 26.5 dB peak gain, 1.4 dB minimum noise figure. Nominal bias levels are V_d = 3.0 V, V_g = 1.5 V, I_d = 26 mA. The in-house manufactured gold-plated copper housing is modeled and displayed mounted in the test dewar in Figure 12. To prepare for cryogenic use, the K-type coaxial connectors have a glass bead, attention was paid to mechanical thermal design, and a thermal bracket is attached for mounting in the test dewar. Room temperature and cryogenic S-parameter and noise temperature tests for various bias settings are performed.

5.2 LNA results

The noise temperature (Figure 13) is measured at 303 K and 13 K using an Agilent N8975A noise figure analyzer with a 14 dB ENR noise source and shows optimum performance around 20 GHz for both cryogenic, 13 K and room temperatures, 303 K. At 303 K the noise temperature is 150 K and the gain is 26 dB at 22 GHz. At 13 K physical temperature, the lowest noise temperature is 20 K at 20 GHz with V_d = 1.5 V, V_g = 0.5 V bias settings, 12.9 mW dissipated but this is also the least gain at cryogenic temperatures, 29 dB. A good compromise is achieved with V_d = 1.5V, V_g = 2.0V, 32.5 mW dissipated with 33 dB gain and 21 K noise temperature at 20 GHz.

Figure 12. LNA. Left: 1x5 LNA Model with top lid removed to show details of single stage MMIC amplifier, transmission lines, bypass capacitors, feed throughs for Vd, Vg, the ground post common to the amplifier body and K-type coaxial connectors. Right: Cryogenic testing; bottom side is thermally mounted to dewar plate, Lakeshore temperature sensor on LNA input calibrated resistor.

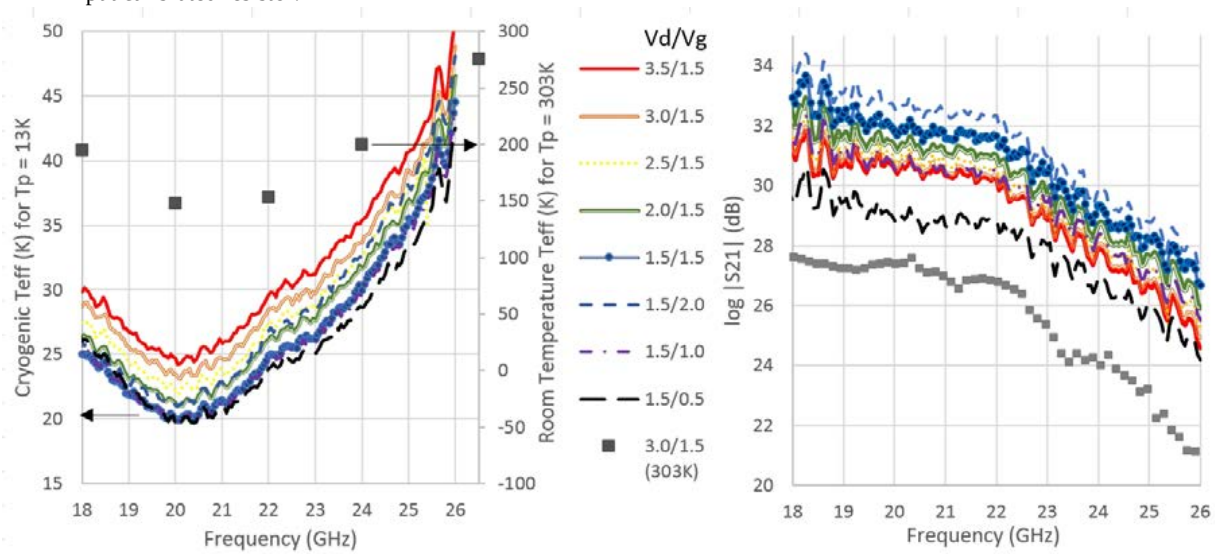

Figure 13. LNA noise temperature and gain as a function of V_d/V_g bias settings at room temperature, 303 K and cryogenic temperature, 13 K.

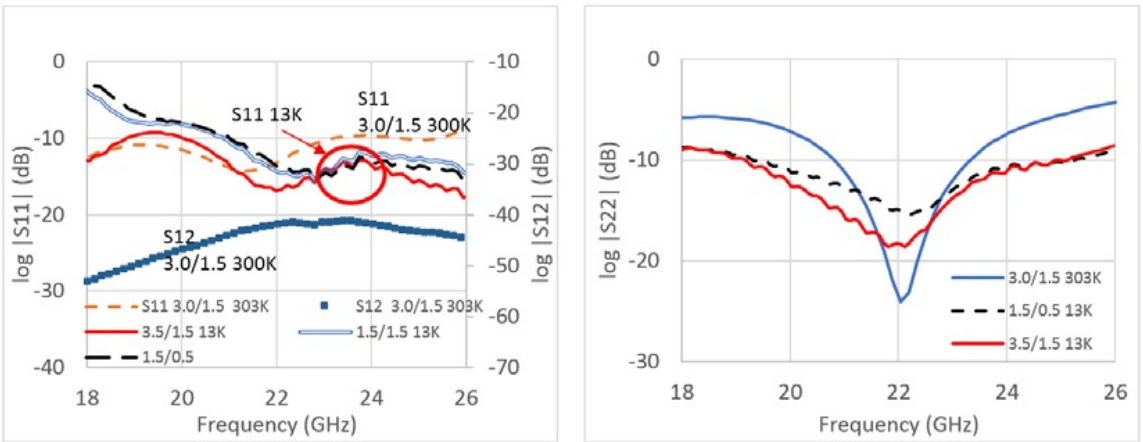

Figure 14. LNA S_{11}, S_{12}, S_{22} as a function of V_d/V_g bias settings at 303 K and 13 K.

The input return loss, reverse isolation and output return loss are shown in Figure 14. S_{12} stays well below -40 dB, performing best at the low end of the band. The best overall S_{11} is attained with a high bias setting of $V_g = 3.5$V, $V_d = 1.5$ V, with a very consistent performance with frequency but slightly better at high frequencies. Both room temperature and cryogenic S_{22} is best at 22 GHz, while staying below -5 dB for room temperature and -9 dB for cryogenic temperatures.

5.3 Mixer description

A down converter for an RF of 18–26 GHz to an IF of 0.8–1.5 GHz is needed to interface with existing instrumentation at NRC Herzberg in Penticton, a baseband mixer and analog beamformer. The K-band mixer design is a packaged Hittite MMIC chip HMC260, a passive double balanced mixer with 50 ohm ports with an added low pass filter on the IF port. The 50 ohm microstrip is on Rogers RT/Duroid 5880 substrate with 5 mil thickness. The LO requires +13 dBm, and we expect 8 to 10 dB conversion loss.

6. PAF SYSTEM

Imaging systems with different number of beams, sensitivities and polarizations can be compared by using survey speed, *SVS*, the imaging speed per unit time assuming uniform gain across the sampled FoV[10].

$$SVS = \frac{\text{FoV}}{t} = \frac{N_{pol} N_b \Omega_b}{t} = N_{pol} N_b \Omega_b B \left(\frac{A_{eff}}{T_{sys}} \right)^2 \tag{2}$$

N_{pol} is the number of independent polarizations, N_b is the number of independent synthesized beams, Ω_b is the solid angle of each beam, t is the time required to sample the image, B is the signal processing bandwidth, A_{eff}/T_{sys} is the antenna sensitivity, A_{eff} is the effective antenna collecting area taking into account efficiencies, and T_{sys} is the system temperature. Given that the antenna spacing is 6.2 mm we expect that an array of 7x7 can synthesize approximately 40 beams (Nyquist spaced and using a hexagonal layout) at 24 GHz at the focal plane of a telescope with an f/D = 0.45. We compare this 40-beam PAF system to a benchmark, a cryogenic dual-polarization SPF, by taking the ratio of the PAF and SPF survey speeds in Figure 15.

The room temperature 40 beam single polarization PAF is worse than the SPF by a factor of 1/0.3 = 3.3. For the PAF to equate the SPF performance, a PAF Tsys of 150 K is needed. Cooling the amplifier while keeping the antenna room temperature results in a performance factor of 2.5 times better than SPF. The greatest factor is seen with an all-cryogenic PAF system, Tsys = 27 K, which is 18 times better than a dual polarization cryogenic SPF.

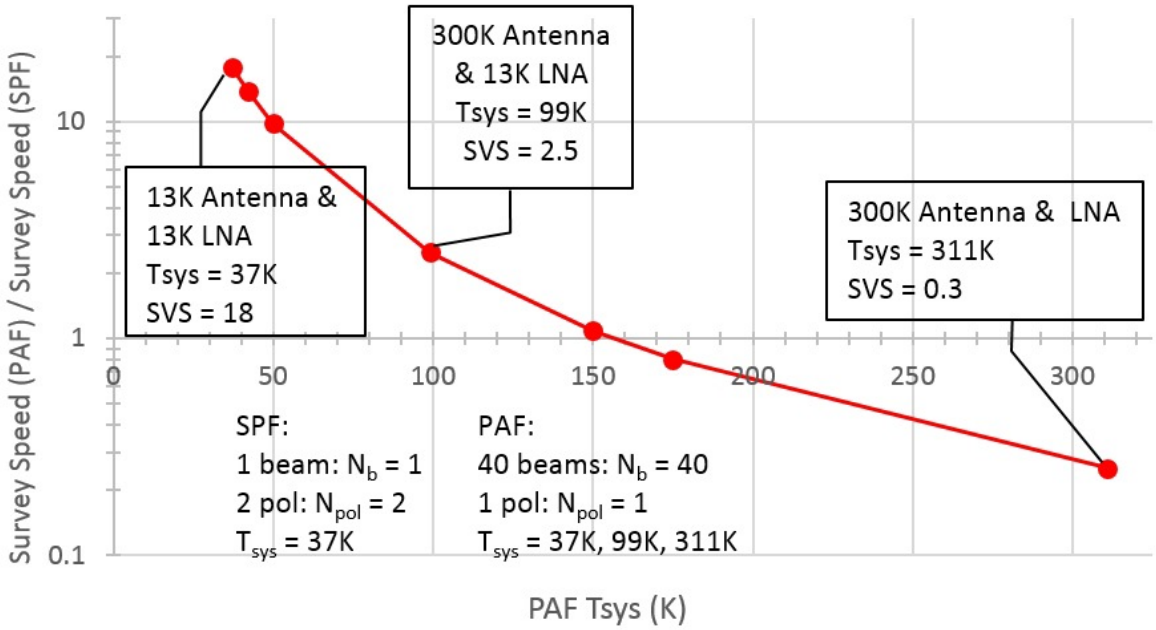

Figure 15. A PAF system normalized to an SPF as given by (2). The SPF is assumed to have dual-linear polarization with a system noise temperature of 37 K. The PAF is assumed to have a single linear polarization and is shown plotted with various physical temperatures of the antenna and LNA. The cryogenic 40 beam PAF is competitive with the cryogenic dual-polarization SPF by a factor of 18.

7. CONCLUSIONS

A K-band 5x5 PAF system including planar TSA elements with SIW feed, cryogenic low-noise amplifier block and mixer assembly for use with a 10 m reflector paraboloid has been designed, and a single blade 1x5 PAF system has been built and tested. Results include full S-parameters and noise temperature estimation. The primary module is proven and future designs will incorporate the modularity of the 5x5 KPAF to create a 10x10 or 15x15 element system. A 40-beam single polarization cryogenic PAF can exceed the performance of a cryogenic SPF by a factor of 18. Future work will incorporate a lower-noise sturdier antenna substrate and a cryogenic integrated antenna-LNA system. PAF systems are quickly becoming a realizable alternative to the single pixel feed.

REFERENCES

[1] Veidt, B., Burgess, T., Yeung, K., Claude, S., Wevers, I., Halman, M., Niranjanan, P., Yao, C., Jew, A., Henke, D. and Willis, A. G., "Noise performance of a phased-array feed composed of thick Vivaldi elements with embedded low-noise amplifiers," to be presented at General Assembly and Scientific Symposium, URSI, Beijing, (2014).

[2] Woestenburg, E. E. M., Bakker, L. and Ivashina, M. V., "Experimental results for the sensitivity of a low noise aperture array tile for the SKA," IEEE Trans. Antennas Propagat., 60(2), 915-921 (2012).

[3] Janaswamy, R. and Schaubert, D. H., "Analysis of the tapered slot antenna," IEEE Trans. Antennas Propagat., 35(9), 1058-1065 (1987).

[4] Lim, T. G., Ang, H. N., Robertson, I. D. and Weiss, B. L., "Tapered slot antenna using photonic bandgap structure to reduce substrate effects," Electronics Letters, 41(7), 393-394 (2005).

[5] Locke, L.S., Bornemann, J. and Claude, S., "Substrate integrated waveguide-fed tapered slot antenna with smooth performance characteristics over an ultra-wide bandwidth," ACES Journal, 28(5), 454-462 (2013).

[6] Deslandes, D. and Wu, K., "Integrated microstrip and rectuangular waveguide in planar form," IEEE Microwave Wireless Comp. Lett., 11(2), 68-70 (2001).

[7] Fisher, J. and Bradley, R., "Full-sampling focal plane arrays," in Imaging at Radio Through Submillimeter Wavelengths, Astron. Soc. Pac. Conf. J. (G. Mangum and S. Radford, eds.) 217, 11-18 (2000).

[8] Minnett, H. C. and Thomas, B. M., "Fields in the imaging space of symmetrical focusing reflectors," Proc. IEE, 115(10), 1419-1430 (1968).

[9] Hayman, D., Bird, T., Esselle, K. and Hall, P., "Encircled power study of focal plane field for estimating focal plane array size," IEEE AP-S Int. Symp. Dig., 3A, 371-374 (2005).

[10] Cordes, J., "Memo 109: survey metrics," SKA Memo Series, (2007).